

# Coupling light into optical fibres near the diffraction limit

Anthony J. Horton and Joss Bland-Hawthorn

Anglo-Australian Observatory, PO Box 296, Epping, NSW, Australia

## ABSTRACT

The burgeoning field of astrophotonics explores the interface between astronomy and photonics. Important applications include photonic OH suppression at near-infrared wavelengths, and integrated photonic spectroscopy. These new photonic mechanisms are not well matched to conventional multi-mode fibre bundles, and are best fed with single or few-mode fibres. We envisage the largest gains in astrophotonics will come from instruments that operate with single or few mode fibres in the diffraction limited or near diffraction limited regime. While astronomical instruments have largely solved the problem of coupling light into multi-mode fibres, this is largely unexplored territory for few-mode and single-mode fibres. Here we describe a project to explore this topic in detail, and present initial results on coupling light into single and few-mode fibres at the diffraction limit. We find that fibres with as few as  $\sim 5$  guided modes have qualitatively different behaviour to single-mode fibres and share a number of the beneficial characteristics of multi-mode fibres.

**Keywords:** few-mode, fibres, coupling, diffraction limit, astrophotonics, optical and infrared astronomy

## 1. INTRODUCTION

Optical fibres have been in use in astronomical instrumentation for almost 30 years. They were first used for fibre-fed multi-object spectroscopy, which began with the Medusa instrument at Steward Observatory in 1979.<sup>1</sup> The efficiency gains from the ability to observe large numbers of objects at once have made many otherwise impractical scientific programmes possible, including several huge spectroscopic surveys of great importance, for example the 2dF galaxy<sup>2</sup> & QSO<sup>3</sup> redshift surveys and the Sloan Digital Sky Survey spectroscopy component.<sup>4</sup> Another important application is integral field spectroscopy. The first instruments using fibre-based integral field units were constructed in the late 1980s,<sup>5-7</sup> and this is now a well established technique employed by a number of major optical and near infrared instruments (e.g. GMOS,<sup>8</sup> VIMOS,<sup>9</sup> IMACS,<sup>10</sup> CIRPASS<sup>11</sup>). Optical fibres are also in use in astronomical optical interferometers.<sup>12</sup>

The importance of optical fibres in astronomy is set to increase even further with the continuing development of adaptive optics (AO). AO systems are now in place on all the world's largest astronomical telescopes, and advanced multi-conjugate adaptive optics (MCAO) systems are planned for both the current generation of telescopes and all of the proposed Extremely Large Telescopes (ELTs). These MCAO systems will provide large AO-corrected fields of view, and the very large number of spatially resolved elements will make efficient sampling of the focal plane essential.<sup>13</sup> This will require new developments in multi-object spectroscopy systems, deployable integral field units and deployable imaging systems, and optical fibres are well suited to play an important role in all of these. Consequently optical fibres, and in particular optical fibres combined with adaptive optics systems, are extremely important to the future of astronomy.

The majority of fibre-fed instruments so far have been designed for operation under natural seeing conditions, and the relative ease of coupling light into multi-mode fibres (MMFs), especially in the presence of atmospheric aberrations, has led to their exclusive use in instruments to date. Developments in astrophotonics now provide a strong motivation to move away from MMFs, however. Astrophotonics is a broad term used for the astronomical application of a wide range of photonic technology, and this burgeoning field has the potential to revolutionise astronomy. Important examples which is likely to have a significant impact in the near future are integrated photonic spectrographs<sup>14</sup> and OH suppression fibres based on aperiodic fibre Bragg gratings<sup>15</sup> (AFBGs), which

---

Further author information: (Send correspondence to A.J.H.)

A.J.H.: E-mail: ajh@aoa.gov.au, Telephone: +61 2 9372 4892

J.B-H.: E-mail: jbh@aoa.gov.au, Telephone: +61 2 9372 4851

promise to give near infrared instruments sky backgrounds as low or possibly even lower than those seen in the optical. These new devices are capable of greatly benefitting astronomy, however a significant obstacle to realising this potential is the fact that many have been conceived as single-mode devices, meaning that they cannot be fed by conventional MMFs.

The most obvious way to integrate a single-mode photonic device into an instrument is to feed it with a single-mode fibre (SMF), but this approach has its own difficulties. Shaklan & Roddier<sup>12</sup> and Coudé du Foresto et al<sup>16</sup> have shown that the theoretical maximum efficiency with which a stellar image can be coupled into a single mode fibre is  $\sim 80\%$  in the absence of any atmospheric turbulence effects or obstructions in the telescope pupil. When the effect of a reasonable circular central obstruction of 20% of the primary diameter is included this falls to  $\sim 70\%$ , and the presence of atmospheric aberrations further reduces the coupling efficiency in proportion to the Strehl ratio. As a result direct coupling of large telescopes to SMFs in natural seeing is rendered impractical by low efficiencies, while the use of SMFs with AO places strong constraints on the necessary performance of the AO system, both in terms of the average Strehl achieved and its variability (which impacts on calibration).

While the continuing development of AO may allow highly efficient and stable coupling of telescopes to SMFs in the future there is an intermediate approach which should allow the efficient integration of astrophotonic devices now. Though many important devices are single-mode it is in general possible to extend them to operate with a few propagating modes. With OH suppressing fibres, for example, the atmospheric emission lines must be blocked separately for each propagating mode, which can be achieved either with a single, more complex AFBG or by using converters to connect to multiple single-mode AFBGs.<sup>17</sup> An integrated spectrograph can also be made to work with a few modes,<sup>14</sup> at least at low and moderate resolutions. Using modified astrophotonic devices such as these makes it possible to use few mode fibres (FMFs) instead of SMFs. The coupling of light into FMFs is relatively unexplored territory, however as the number of modes increases it will become easier to couple light into the fibres, which is expected to reduce the sensitivity to AO system performance at the expense of increasing the required complexity of attached astrophotonic devices. Indeed for some, such as OH suppression fibres, it will be practical to use sufficiently many modes to allow use under natural seeing. In this paper we describe an ongoing investigation into the trade off between coupling efficiency and the number of propagating modes.

## 2. THEORY

### 2.1. Fibre Modes

The multi-mode fibres typically used in astronomical instruments, whose core radii are much greater than the operating wavelength, can in many ways be regarded as ‘light pipes’, and their properties predicted with reasonable accuracy using geometric optics methods. If the size of the fibre core is less than  $\sim 50$  times the wavelength, however, the geometric optics approximation breaks down and it becomes necessary to treat the fibre as a dielectric waveguide and solve for the electromagnetic fields of the propagating modes. The behaviour of the fibre can then be predicted from the characteristics of the individual modes. In this investigation we have followed the treatments of Gloge,<sup>18</sup> Midwinter<sup>19</sup> and Jeunhomme.<sup>20</sup>

We consider a conventional silica step-index fibre, consisting of a core of radius  $a$  with uniform refractive index  $n_1$  surrounding by cladding material of uniform index  $n_2 < n_1$ . In the limit of  $\Delta = (n_1 - n_2)/n_2 \ll 1$  the propagating modes of such a fibre have a particularly simple form. In this ‘weakly-guiding’ limit the Maxwell equations can be transformed into a scalar wave equation for the longitudinal components, and the fields within the fibre expressed as a series of linearly polarised (LP) modes. In practice this is a reasonable approximation for a real fibre, as the difference in refractive indices is generally  $< 1\%$  and the resulting error in mode characteristics  $< 0.1\%$ .

The LP modes are characterised by two numbers, the azimuthal order,  $l$ , and the radial order,  $m$ . The transverse component of the electric field of the  $LP_{lm}$  mode is given by

$$E_{lm}(\rho, \theta) = A_{lm} (\sin l\theta, \cos l\theta) J_l(u_{lm}\rho) / J_l(u_{lm}) \quad \rho \leq 1 \quad (1)$$

$$A_{lm} (\sin l\theta, \cos l\theta) K_l(w_{lm}\rho) / K_l(w_{lm}) \quad \rho > 1, \quad (2)$$

**Table 1.** Cutoff frequencies for the linearly polarised modes of a step index fibre.

$l$	$m$	$V_c$	$l$	$m$	$V_c$	$l$	$m$	$V_c$	$l$	$m$	$V_c$
0	1	0.000	4	1	6.380	6	1	8.771	5	2	11.065
1	1	2.405	0	3	7.016	4	2	9.761	8	1	11.619
0	2	3.832	2	2	7.016	7	1	9.936	1	4	11.792
2	1	3.832	5	1	7.588	0	4	10.173	9	1	12.225
3	1	5.136	3	2	8.417	2	3	10.173	6	2	12.339
1	2	5.520	1	3	8.654	3	3	11.086	4	3	13.015

where  $\rho$  is the normalised radial coordinate  $r/a$ ,  $J_l$  is the Bessel function of the first kind of order  $l$  and  $K_l$  is corresponding modified Bessel function of the second kind. For each LP mode with  $l \neq 0$  two independent orientations exist, with  $\sin l\theta$  and  $\cos l\theta$  azimuthal dependences. The longitudinal components are small compared to the transverse (by a factor  $> 1/\sqrt{2\Delta}$ ) and can for most purposes be neglected.

The transverse propagation constants for the core ( $u_{lm}$ ) and cladding ( $w_{lm}$ ) are determined by the normalised frequency,  $V$ , which is defined by  $V = 2\pi a \text{NA}/\lambda$  where  $\lambda$  is wavelength and  $\text{NA} = \sqrt{n_1^2 - n_2^2} \approx n_2 \sqrt{2\Delta}$  is the numerical aperture of the fibre. The transverse propagation constants satisfy

$$V = \sqrt{u^2 + w^2} \quad (3)$$

and  $u_{lm}, w_{lm}$  are given by the  $m$ th root of

$$u \frac{J_{l-1}(u)}{J_l(u)} + w \frac{K_{l-1}(w)}{K_l(w)} = 0. \quad (4)$$

From Eqs. (3) and (4) it can be shown that  $u_{lm}$  must lie between the  $m$ th zero of  $J_{l-1}$  and the  $m$ th zero of  $J_l$ . For a mode to be guided by the fibre  $w_{lm}$  must be real, and so the minimum value of  $u_{lm}$  defines the cutoff frequency,  $V_c$ , for the mode. In the special case of  $l = 0$  the  $m = 1$  mode has a cutoff frequency of zero, this is the fundamental mode of the fibre and is always present. For a more rigorous treatment of the cutoff conditions see, for example, Marcuse.<sup>21</sup> The cutoff frequencies of the first few LP modes are given in Table 1. As can be seen from the table the cutoff frequencies of the LP modes become more closely spaced at higher frequencies, in fact the number of guided modes at a normalised frequency  $V$  is approximately proportional to  $V^2$ .

## 2.2. Image Field

The field distribution in the focal plane of a telescope is related to the distribution in the entrance pupil by

$$\mathbf{E}_{\text{focus}}(\mathbf{r}) \propto \tilde{\mathbf{E}}_{\text{pupil}}\left(\frac{\mathbf{r}}{\lambda f}\right) \quad (5)$$

where the tilde represents a Fourier transform and  $f$  is the effective focal length of the telescope. The field in the entrance pupil can be written as

$$\mathbf{E}_{\text{pupil}}(\mathbf{r}') = \mathbf{E}_* P(\mathbf{r}') \Psi(\mathbf{r}') \quad (6)$$

where  $\mathbf{E}_*$  is the field received from the source,  $P$  is the pupil transmission function and  $\Psi$  is a phase screen which incorporates any optical aberrations, either fixed aberrations inherent to the telescope optics or random, variable aberrations due to passage of the incoming light through turbulence in the atmosphere.

Initially we consider the diffraction limited case where there are no aberrations, i.e.  $\Psi = 1$ . If we represent the telescope pupil as a circular aperture of radius  $R$  with a central obstruction of radius  $\alpha R$  then the focal plane field distribution for a point source is given by

$$\mathbf{E}_{\text{focus}} = \mathbf{E}_0 \left[ \frac{2J_1(s)}{s} - \alpha^2 \frac{2J_1(\alpha s)}{\alpha s} \right] \quad (7)$$

where  $s$  is a scaled radial coordinate given by  $s = 2\pi Rr/\lambda f$ . Noting that  $2R/f$  is the definition of focal ratio of the telescope,  $F$ , we see that the dimensions of the diffraction limited image scale in proportion to the product  $\lambda F$ .

### 2.3. Coupling Efficiency

The fraction of incident energy which is coupled into an individual mode,  $\epsilon_{lm}$ , can be calculated from the electric field distribution of the image  $E_{\text{focus}}$  and that of the fibre mode  $E_{lm}$  according to

$$\epsilon_{lm} = \frac{\left| \int_{\infty} \mathbf{E}_{\text{focus}}^* \cdot \mathbf{E}_{lm} dA \right|^2}{\int_{\infty} |\mathbf{E}_{\text{focus}}|^2 dA \int_{\infty} |\mathbf{E}_{lm}|^2 dA}. \quad (8)$$

The asterisk indicates complex conjugation and the integrals are performed over an infinite plane at the telescope focus. When ignoring polarisation and by noting that the electric field of the incident light is purely transverse we can rewrite Eq. (8) in terms of inner products of the transverse field component distributions, i.e.

$$\epsilon_{lm} = \frac{|\langle E_{\text{focus}} | E_{lm} \rangle|^2}{\langle E_{\text{focus}} | E_{\text{focus}} \rangle \langle E_{lm} | E_{lm} \rangle} \quad (9)$$

where  $E_{\text{focus}}$  is the scalar part of Eq. 7 and  $E_{lm}$  is the transverse component of the  $\text{LP}_{lm}$  mode field as in Eqs. (1) and (2). In writing Eq. (9) we have also used the fact that the longitudinal field components of an LP mode are small relative to the transverse components (see Sect. 2.1) to neglect their contribution to  $\int_{\infty} |\mathbf{E}_{lm}|^2 dA$ .

The coupling efficiency  $\epsilon$ , defined as the fraction of the incident energy which ends up being guided by the fibre, is simply given by summing the  $\epsilon_{lm}$  over all the guided modes.

## 3. INITIAL RESULTS

### 3.1. Model System

In the calculations described here we use diffraction limited images coupled directly into a step index fibre in the focal plane. Such a system can be characterised by three dimensionless parameters,  $S$ ,  $\alpha$  and  $V$ . The parameter  $S = \lambda F/a$  determines the scale of the image relative to the fibre core, the central obstruction size  $\alpha$  determines the form of the image, and the normalised frequency  $V = 2\pi a \text{NA}/\lambda$  determines the number and form of the guided modes. However instead of presenting our results in terms of these generalised parameters we prefer to work with the more physical set of variables  $F$ ,  $\alpha$  and  $d = 2a$ , and assume appropriate values for  $\lambda$  and NA. The results can of course be transformed to other wavelengths or NAs via the corresponding values of  $S$  and  $V$ .

The wavelengths and NA used have been chosen to be representative of likely values for an astrophotonics application. The H-band wavelength region is of particular interest as this is the region being targeted by the first generation of OH suppression AFBGs, and FMF coupling will play an important role in integrating these devices into full scale astronomical instruments. For this reason we have used H-band wavelengths in these calculations, selecting  $1.5\mu\text{m}$  as representative. Ordinary silica optical fibres typically have numerical apertures in the range 0.1–0.2, with SMFs generally towards the lower end of this range and MMFs higher. For these calculations we have used an NA of 0.1.

### 3.2. Maximum Coupling Efficiency Versus Core Diameter

The first result from these investigations was the dependence of maximum coupling efficiency on the fibre core diameter. To calculate this the coupling efficiency was optimised against focal ratio for core diameters in the range  $5\text{--}60\mu\text{m}$ . For  $\lambda = 1.5\mu\text{m}$  and  $\text{NA} = 0.1$  this range of core diameters corresponds to a range in normalised frequency of 1.05–12.6, which as can be seen from Table 1 covers single mode operation at the lower end ( $d < 11.5\mu\text{m}$ ) up to 23 guided modes at the upper limit.

The results are shown in Fig. 1(a) and Fig. 1(b) for  $\alpha = 0$  and  $\alpha = 0.2$  respectively. The two values of  $\alpha$  represent the ideal case and one more typical of the current generation of large telescopes. In both cases there is a monotonic increase in total coupling efficiency as the core diameter increases (from 67% to 94% for  $\alpha = 0$ , 58% to

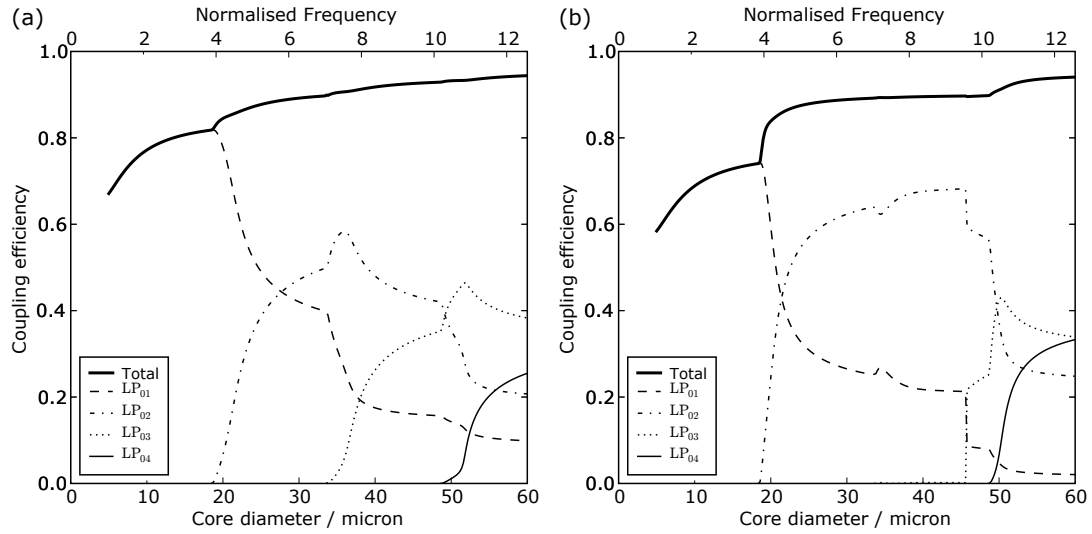


**Figure 1.** Maximum coupling efficiency versus core diameter for an  $NA = 0.1$  fibre at a wavelength of  $1.5\mu\text{m}$ . The overall coupling efficiency and the contributions from each fibre mode are shown for (a)  $\alpha = 0$  and (b)  $\alpha = 0.2$ .

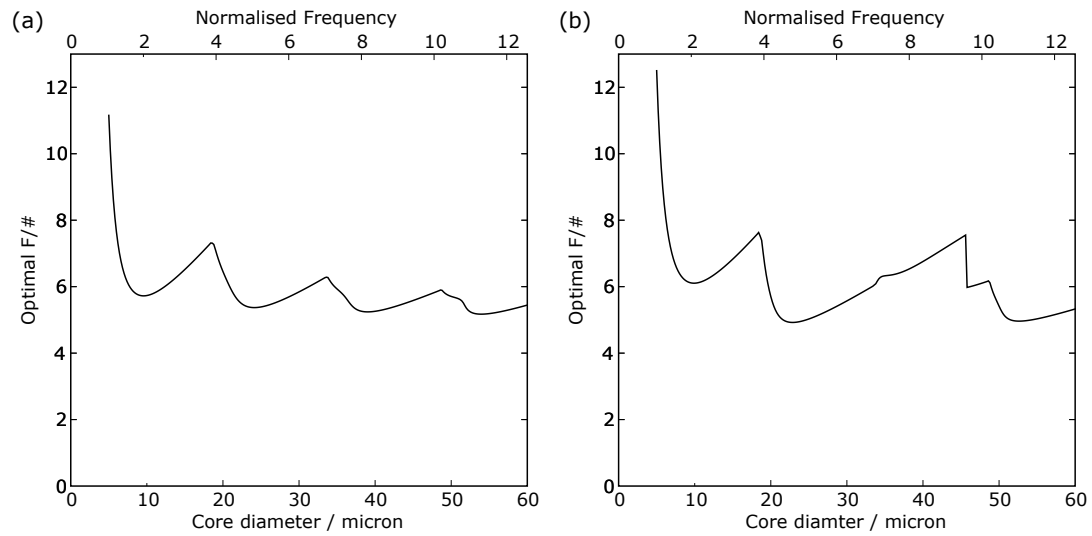


**Figure 2.** Optimal focal ratio versus core diameter for an  $NA = 0.1$  fibre at a wavelength of  $1.5\mu\text{m}$ . The focal ratio corresponding to maximum coupling efficiency is shown for (a)  $\alpha = 0$  and (b)  $\alpha = 0.2$ .

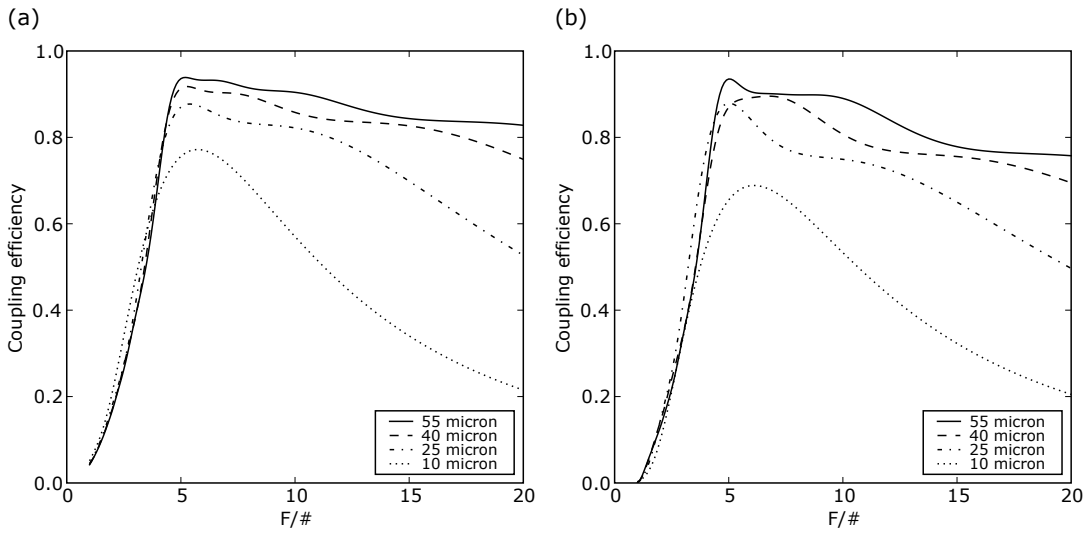


**Figure 3.** Coupling efficiency versus focal ratio for an  $NA = 0.1$  fibre at a wavelength of  $1.5\mu\text{m}$ . Coupling efficiency is shown for core diameters of 10, 25, 40 and  $55\mu\text{m}$  with (a)  $\alpha = 0$  and (b)  $\alpha = 0.2$ .

94% for  $\alpha = 0.2$ ) punctuated by a number of discontinuities in the gradient. From these results we immediately see that FMFs give significantly higher maximum coupling efficiency than SMFs ( $d < 11.5\mu\text{m}$ ), especially in the more realistic  $\alpha = 0.2$  case. The cause of the discontinuities becomes apparent when the contributions from each of the guided modes are examined so these have also been plotted on Fig. 1. In this calculation the image is aligned with the fibre axis and due to the axial symmetry only  $l = 0$  modes contribute. In the  $\alpha = 0$  case the position of the discontinuities coincides with the cutoff frequencies of the  $LP_{02}$ ,  $LP_{03}$  and  $LP_{04}$  modes, and it is the appearance of these modes that provides a boost to the coupling efficiency. The  $\alpha = 0.2$  case is slightly more complex as the different image profile results in significant jumps in coupling efficiency at the appearance of the  $LP_{02}$  and  $LP_{04}$  modes while the  $LP_{03}$  mode does not contribute until well above its cutoff.

The significant negative effect on SMF coupling efficiency of a central obstruction in the telescope pupil was previously noted by Coude du Foresto et al.<sup>16</sup> and a comparison of the small core diameter ends of Fig. 1(a) and Fig. 1(b) shows that an efficiency loss of  $\sim 10\%$  occurs with  $\alpha = 0.2$ . The effect of the central obstruction on the image is to reduce the field strength in the central peak while increasing it in the first ring, which reduces the coupling to the  $LP_{01}$  mode. This change in image profile increases the coupling to the  $LP_{02}$  mode, however, and so above the  $LP_{02}$  cutoff we see the maximum coupling efficiency for  $\alpha = 0.2$  approximately equal that for  $\alpha = 0$ . Similarly the  $\alpha = 0.2$  image does not couple well to the  $LP_{03}$  mode, but does to  $LP_{04}$ .

### 3.3. Focal Ratio Dependence

In calculating the maximum coupling efficiency as a function of core diameter we also obtained the focal ratios at which maximum coupling efficiency is achieved. These optimal focal ratios are shown in Figs. 2(a) and 2(b) for the  $\alpha = 0$  and  $\alpha = 0.2$  cases. To get a fuller picture of the effect of focal ratio we also calculated coupling efficiency for  $F = 1\text{--}20$  for four core diameters of 10, 25, 40,  $55\mu\text{m}$ . With  $NA = 0.1$  and  $\lambda = 1.5\mu\text{m}$  these core diameters have one, two, three and four guided  $l = 0$  modes respectively. The results for  $\alpha = 0$  and  $\alpha = 0.2$  are plotted as Fig. 3(a) and Fig. 3(b).

The mode cutoffs and changes in the contributions of each mode seen in Fig. 1 are also seen reflected in variations in the optimal focal ratio in Fig. 2, however as the diameter increases the variations diminish and the optimal focal ratio converges from above on a value of  $\sim 5$ . In other words the optimal image size does not scale with the fibre diameter but instead remains relatively constant. Looking at Fig. 3 we see that for all the plotted core diameters the coupling efficiency declines rapidly for focal ratios less than  $\sim 5$ . This low

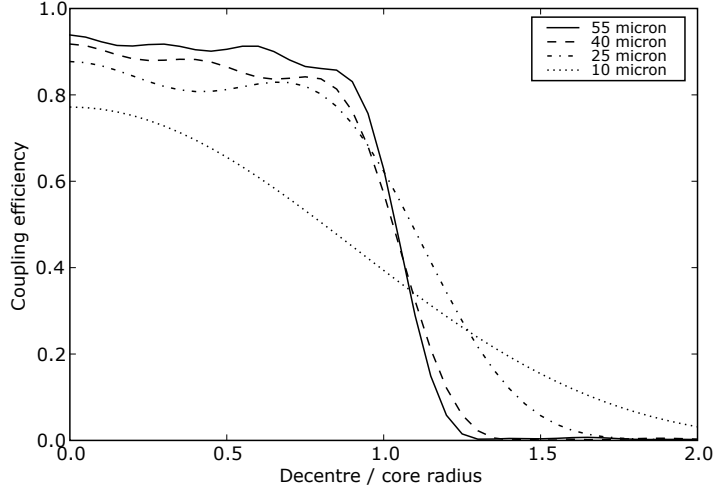


**Figure 4.** Coupling efficiency versus decentring of the image centre from the fibre axis. Coupling efficiency is shown for  $NA = 0.1$  fibres with 10, 25, 40 and  $55\mu\text{m}$  core diameters at a wavelength of  $1.5\mu\text{m}$  and with  $\alpha = 0$ .

$F$  cutoff is the same as predicted in the multi-mode limit via geometric optics. By considering the condition for total internal reflection to occur at the core/cladding interface the numerical aperture of the fibre can be equated to the sine of the maximum angle of incidence at which a light ray can strike the fibre face and still be guided within the core. This maximum angle can then be converted into a minimum focal ratio via  $F_{\min} = 1/2 \tan(\sin^{-1} NA) \approx 1/(2NA)$ , and for an  $NA$  of 0.1 this is 4.97. So we see that the geometric optics derived maximum focal ratio for MMFs also applies to the single and few-mode regime, and furthermore the optimum focal ratio for FMFs lies close to this value.

The other main feature of Fig. 3 is the decreasing sensitivity of the coupling efficiency to higher than optimum focal ratios as the core diameter increases. This would be intuitively expected as the larger core allows for greater magnification of the image (higher  $F$ ) before a significant proportion of the light falls outside the core. Upon examining the contributions of the individual modes as the focal ratio changes it is also possible to explain a number of the features in the coupling efficiency slope, which are particularly apparent in the  $\alpha = 0.2$  case. As the focal ratio increases the lower order modes become progressively more important and so, for instance, the significant decline in coupling efficiency between  $F = 5$  and  $F = 7$  for a  $25\mu\text{m}$  core when  $\alpha = 0.2$  is due to a decline in the  $LP_{02}$  mode and a transition to dominance by the poorly coupling  $LP_{01}$  mode. The other features can be similarly ascribed to the decline of particular modes.

### 3.4. Sensitivity to Decentring

While the increases seen in maximum coupling efficiency with only a few additional modes are pleasing, the primary motivation for undertaking this investigation is the expectation that FMF coupling efficiency will be considerably less sensitive than SMFs to deviations from ideal conditions, thereby making them a more practical option for real world applications. In order to determine to what extent this is true we must calculate the effect of realistic aberrations on the coupling efficiency. However, at the time of writing, the only aspect of this analysis which is complete is an examination of the effect of displacing the image centre from the fibre axis. Such displacements are certain to occur to some degree in astronomical use for a number of reasons such as imperfect correction of wavefront tip/tilt, finite fibre positioner precision and finite accuracy of astrometry.

Figure 4 shows the coupling efficiency as a function of image decentring for 10, 25, 40 and  $55\mu\text{m}$  diameter cores. For these calculations there is no axial symmetry and so all the guided modes must be included, not just the  $l = 0$  ones. With  $NA = 0.1$  and  $\lambda = 1.5\mu\text{m}$  the four core diameters give 1, 5, 10 and 19 guided modes respectively. The previously calculated focal ratios for maximum (on-axis) coupling efficiency were used for each

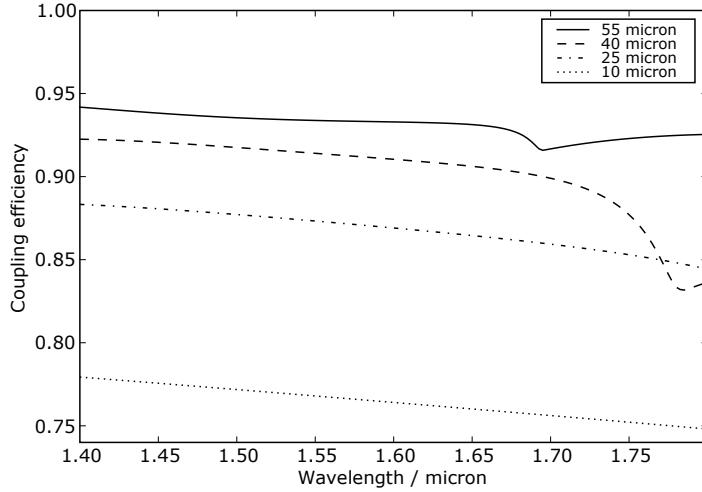


**Figure 5.** Coupling efficiency versus wavelength for  $NA = 0.1$  fibres with core diameters of 10, 25, 40 and  $55\mu\text{m}$ , and with  $\alpha = 0$ . For each diameter the focal ratio was fixed at the optimal value for a wavelength of  $1.6\mu\text{m}$ .

diameter. For simplicity only the  $\alpha = 0$  case is shown, but the  $\alpha = 0.2$  results are similar. There is a qualitative difference in behaviour here between SMFs and FMFs, whereas fibres with 5 or more modes show variations in coupling efficiency of only  $\sim 5\%$  for decentres up to 80% of the core radius the single-mode fibre loses over a third of its coupling efficiency over the same range. This flat response is a desirable property of the FMFs as it means that moderate image-fibre misalignments will not cause drops in throughput and attendant calibration issues.

Knowing the dependence of point source coupling efficiency on image position also enables us to calculate the coupling efficiency for an extended source. For an extended source with an angular intensity distribution on the sky of  $I_{\text{ext}}(\theta)$  the effective coupling efficiency  $\epsilon_{\text{ext}}$  is given by

$$\epsilon_{\text{ext}} = \frac{\int_{\infty} \epsilon_{\text{psf}}(\mathbf{r}) I_{\text{ext}}(\mathbf{r}/f) dA}{\int_{\infty} I_{\text{ext}}(\mathbf{r}/f) dA} \quad (10)$$

where  $\epsilon_{\text{psf}}(\mathbf{r})$  is the coupling efficiency for a point source image centred on a position  $\mathbf{r}$  in the focal plane. This is in effect taking a weighted average of the coupling efficiency over the area of the source image, and so while the exact figure will depend on the shape and size of the source what can be said is that the flatter responses seen with the FMFs will further increase their coupling efficiency advantage over SMFs for resolved sources.

We can also calculate the effective solid angle of sky coupled into the fibre,  $\Omega_{\text{sky}} = \pi(a/f)^2 \int_{\infty} \epsilon_{\text{psf}} dA$ . For the core diameters considered here we find  $\int_{\infty} \epsilon_{\text{psf}} dA \approx 1$  (0.98, 1.10, 0.93 and 0.96) and so  $\Omega_{\text{sky}} \approx \pi D^2 (a/F)^2$ , the same result as would be derived from geometric optics. This strong dependence of the sky background on  $(a/F)^2$  together with the previously established relative insensitivity of FMF coupling efficiency to increasing  $F$  (see Fig. 3) means that the focal ratio which maximises signal-to-noise ratio will in general be larger than the optimal value for coupling efficiency, and except for very bright sources will be that which matches the scale of the source image to the core size, the same as for the MMFs.

### 3.5. Wavelength Dependence

The previous calculations have been performed for a single wavelength, however astronomical applications generally require good performance over a wide wavelength range. Figure 5 shows coupling efficiency as a function of wavelength for  $NA = 0.1$  fibres with core diameters of 10, 25, 40 and  $55\mu\text{m}$ . For each diameter the focal ratio was fixed at the optimal value for  $1.6\mu\text{m}$  while the wavelength was varied over the range  $1.4\text{--}1.8\mu\text{m}$ . This

wavelength range encompasses the whole of the  $\sim 1.45\text{--}1.75\mu\text{m}$  H-band, which is of particular interest due to its connection with OH suppression fibre developments. Only  $\alpha = 0$  results are shown, but  $\alpha = 0.2$  is similar. The general trend for all core diameters is a gradual decrease in coupling efficiency of  $\sim 3\%$  over the wavelength range, however for the  $40$  and  $55\mu\text{m}$  core diameters there is a significant dip superimposed on this steady decline. For the  $40\mu\text{m}$  core this feature corresponds to the  $\text{LP}_{03}$  mode cutoff, while for  $55\mu\text{m}$  the  $\text{LP}_{04}$  mode cutoff is the cause. So we see that in general SMFs and FMFs exhibit good broadband performance, however it would be best to chose fibre parameters so as to avoid an  $l = 0$  mode cutoff falling within an operational wavelength band.

#### 4. DISCUSSION

Astrophotonic developments such as OH suppression fibres and integrated photonic spectrographs have enormous potential, however efficiently integrating them into an astronomical instrument presents a challenge. The MMFs conventionally used in astronomy, while efficient at accepting starlight, are not suitable for feeding light into these devices as the devices are not able to accept a large number of modes. SMFs, on the other hand, while ideal for feeding light into astrophotonic devices are difficult to couple starlight into, even with adaptive optics. We have begun an investigation into the intermediate territory of FMFs, in order to find the best compromise between the two extremes.

Our initial results on diffraction limited fibre coupling have shown that FMFs exhibit many of the desirable properties of MMFs even when there are only of order 10 guided modes. For example, FMFs offer higher maximum coupling efficiency than SMFs ( $> 90\%$ ), especially for extended sources. Also FMFs are less sensitive to the effects of obstructions in the telescope pupil than SMFs are. Unlike SMFs, FMFs can efficiently couple light over a range of focal ratios from  $F_{\min} \approx 1/(2.\text{NA})$  up to a maximum value determined by matching the size of the image to the fibre core. FMFs are also tolerant of displacement of the image centre from the fibre axis, provided the image remains within the fibre core. Both SMFs and FMFs exhibit little sensitivity to wavelength.

While these results are encouraging the use of perfect diffraction limited images does represent an idealised case. In any real ground based telescope the adaptive optics correction will be imperfect, and the residual atmospheric wavefront perturbations will effect the coupling efficiency. It is known that SMF coupling is highly sensitive to imperfect correction, with the coupling efficiency declining in proportion to the Strehl ratio,<sup>16</sup> however the corresponding dependency for FMFs has not yet been investigated. At the time of writing simulated partially corrected atmospheric phase screens were being included in the model system to investigate the effects of various levels of aberrations on fibre coupling performance. The aim of this work is to determine the dependence of FMF coupling efficiency on the order of correction, from natural seeing to the diffraction limit, and thereby establish the number of modes required for acceptable throughput levels under a range of realistic usage conditions.

Preliminary results have also been obtained for pupil-plane coupling to FMFs, which show a similar rapid convergence on MMF behaviour above  $\sim 10$  modes as the image-plane results discussed here. This work will be extended to model lenslet arrays of various geometries and both image and pupil-plane coupling with a view to determining the best approach for FMF integral field spectroscopy.

#### ACKNOWLEDGMENTS

The authors gratefully acknowledge the support of PPARC research grant PP/D002494/1 for this programme of work.

#### REFERENCES

1. J. M. Hill, J. R. P. Angel, J. S. Scott, D. Lindley, and P. Hintzen, “Multiple object spectroscopy - The Medusa spectrograph,” *ApJ* **242**, pp. L69–L72, Dec. 1980.
2. M. Colless, G. Dalton, S. Maddox, W. Sutherland, P. Norberg, S. Cole, J. Bland-Hawthorn, T. Bridges, R. Cannon, C. Collins, W. Couch, N. Cross, K. Deeley, R. De Propris, S. P. Driver, G. Efstathiou, R. S. Ellis, C. S. Frenk, K. Glazebrook, C. Jackson, O. Lahav, I. Lewis, S. Lumsden, D. Madgwick, J. A. Peacock, B. A. Peterson, I. Price, M. Seaborne, and K. Taylor, “The 2dF Galaxy Redshift Survey: spectra and redshifts,” *MNRAS* **328**, pp. 1039–1063, Dec. 2001.

3. S. M. Croom, R. J. Smith, B. J. Boyle, T. Shanks, L. Miller, P. J. Outram, and N. S. Loaring, “The 2dF QSO Redshift Survey - XII. The spectroscopic catalogue and luminosity function,” *MNRAS* **349**, pp. 1397–1418, Apr. 2004.
4. D. G. York, J. Adelman, J. E. Anderson, S. F. Anderson, J. Annis, N. A. Bahcall, J. A. Bakken, R. Barkhouser, S. Bastian, E. Berman, W. N. Boroski, S. Bracker, C. Briegel, J. W. Briggs, J. Brinkmann, R. Brunner, S. Burles, L. Carey, M. A. Carr, F. J. Castander, B. Chen, P. L. Colestock, A. J. Connolly, J. H. Crocker, I. Csabai, P. C. Czarapata, J. E. Davis, M. Doi, T. Dombeck, D. Eisenstein, N. Ellman, B. R. Elms, M. L. Evans, X. Fan, G. R. Federwitz, L. Fiscelli, S. Friedman, J. A. Frieman, M. Fukugita, B. Gillepie, J. E. Gunn, V. K. Gurbani, E. de Haas, M. Haldeman, F. H. Harris, J. Hayes, T. M. Heckman, G. S. Hennessy, R. B. Hindsley, S. Holm, D. J. Holmgren, C.-h. Huang, C. Hull, D. Husby, S.-I. Ichikawa, T. Ichikawa, Ž. Ivezić, S. Kent, R. S. J. Kim, E. Kinney, M. Klaene, A. N. Kleinman, S. Kleinman, G. R. Knapp, J. Korienek, R. G. Kron, P. Z. Kunszt, D. Q. Lamb, B. Lee, R. F. Leger, S. Limmongkol, C. Lindenmeyer, D. C. Long, C. Loomis, J. Loveday, R. Lucinio, R. H. Lupton, B. MacKinnon, E. J. Mannery, P. M. Mantsch, B. Margon, P. McGeehee, T. A. McKay, A. Meiksin, A. Merelli, D. G. Monet, J. A. Munn, V. K. Narayanan, T. Nash, E. Neilsen, R. Neswold, H. J. Newberg, R. C. Nichol, T. Nicinski, M. Nonino, N. Okada, S. Okamura, J. P. Ostriker, R. Owen, A. G. Pauls, J. Peoples, R. L. Peterson, D. Petravick, J. R. Pier, A. Pope, R. Pordes, A. Prosapio, R. Rechenmacher, T. R. Quinn, G. T. Richards, M. W. Richmond, C. H. Rivetta, C. M. Rockosi, K. Ruthmansdorfer, D. Sandford, D. J. Schlegel, D. P. Schneider, M. Sekiguchi, G. Sergey, K. Shimasaku, W. A. Siegmund, S. Smee, J. A. Smith, S. Snedden, R. Stone, C. Stoughton, M. A. Strauss, C. Stubbs, M. SubbaRao, A. S. Szalay, I. Szapudi, G. P. Szokoly, A. R. Thakar, C. Tremonti, D. L. Tucker, A. Uomoto, D. Vanden Berk, M. S. Vogeley, P. Waddell, S.-I. Wang, M. Watanabe, D. H. Weinberg, B. Yanny, and N. Yasuda, “The Sloan Digital Sky Survey: Technical Summary,” *AJ* **120**, pp. 1579–1587, Sept. 2000.
5. J. Guerin and P. Felenbok, “Optical fibres for astronomical applications,” in *Fiber Optics in Astronomy*, S. C. Barden, ed., *ASP Conf. Ser.* **3**, pp. 52–62, 1988.
6. C. Vanderriest, “Integral Field spectrography with Optical Fibres at C.F.H.,” in *Fiber Optics in Astronomy II*, P. M. Gray, ed., *ASP Conf. Ser.* **37**, pp. 338–+, Jan. 1993.
7. S. C. Barden and R. A. Wade, “DensePak and spectral imaging with fiber optics,” in *Fiber Optics in Astronomy*, S. C. Barden, ed., *ASP Conf. Ser.* **3**, pp. 113–124, 1988.
8. J. Allington-Smith, G. Murray, R. Content, G. Dodsworth, R. Davies, B. W. Miller, J. Turner, I. Jorgensen, I. Hook, D. Crampton, and R. Murowinski, “The GMOS Integral Field Unit: First Integral Field Spectroscopy with an 8m Telescope (Invited Talk),” in *Galaxies: the Third Dimension*, M. Rosada, L. Binette, and L. Arias, eds., *ASP Conf. Ser.* **282**, pp. 415–+, Jan. 2002.
9. O. Le Fevre, M. Saisse, D. Mancini, G. P. Vettolani, D. Maccagni, J. P. Picat, Y. Mellier, A. Mazure, J. G. Cuby, B. Delabre, B. Garilli, L. Hill, E. Prieto, C. Voet, L. Arnold, S. Brau-Nogue, E. Cascone, P. Conconi, G. Finger, G. Huster, A. Lalage, C. Lucuix, E. Mattaini, P. Schipani, G. Waultier, F. M. Zerbi, G. Avila, J. W. Beletic, S. D’Odorico, A. F. Moorwood, G. J. Monnet, and J. Reyes Moreno, “VIMOS and NIRIMOS multi-object spectrographs for the ESO VLT,” in *Optical and IR Telescope Instrumentation and Detectors*, M. Iye and A. F. Moorwood, eds., *Proc. SPIE* **4008**, pp. 546–557, Aug. 2000.
10. J. Schmoll, G. N. Dodsworth, R. Content, and J. R. Allington-Smith, “Design and construction of the IMACS-IFU: a 2000-element integral field unit,” in *Ground-based Instrumentation for Astronomy*, A. F. M. Moorwood and M. Iye, eds., *Proc. SPIE* **5492**, pp. 624–633, Sept. 2004.
11. I. Parry, A. Bunker, A. Dean, M. Doherty, A. Horton, D. King, M. Lemoine-Busserole, C. D. Mackay, R. McMahon, S. Medlen, R. G. Sharp, and J. Smith, “CIRPASS: description, performance, and astronomical results,” in *Ground-based Instrumentation for Astronomy*, A. F. M. Moorwood and M. Iye, eds., *Proc. SPIE* **5492**, pp. 1135–1144, Sept. 2004.
12. S. Shaklan and F. Roddier, “Coupling starlight into single-mode fibre optics,” *Appl. Opt.* **27**, pp. 2334–2338, June 1988.
13. J. Bland-Hawthorn, “In search of first light: New technologies and new ideas,” *New Astronomy Review* **50**, pp. 75–83, Mar. 2006.

14. J. Bland-Hawthorn and A. J. Horton, "Instruments without optics: an integrated photonic spectrograph," in *Ground-based and Airborne Instrumentation for Astronomy*, I. S. McLean and M. Iye, eds., *Proc. SPIE* **6269**, Paper 23, 2006.
15. J. Bland-Hawthorn, M. Englund, and G. Edvell, "New approach to atmospheric OH suppression using an aperiodic fibre Bragg grating," *Opt. Express* **12**, pp. 5902–5909, 2004.
16. V. Coudé du Foresto, M. Faucherre, N. Hubin, and P. Gitton, "Using single-mode fibers to monitor fast Strehl ratio fluctuations. Application to a 3.6 m telescope corrected by adaptive optics," *A&AS* **145**, pp. 305–310, Aug. 2000.
17. S. G. Leon-Saval, T. A. Birks, J. Bland-Hawthorn, and M. Englund, "Multimode fiber devices with single-mode performance," *Opt. Lett.* **30**, pp. 2545–2547, 2005.
18. D. Gloge, "Weakly guiding fibres," *Appl. Opt.* **10**, pp. 2252–2258, October 1971.
19. J. E. Midwinter, *Optical Fibres for Transmission*, Wiley, New York, 1979.
20. L. B. Jeunhomme, *Single-Mode Fibre Optics*, Marcel Dekker, New York, 1983.
21. D. Marcuse, *Theory of dielectric optical waveguides*, Academic Press, New York, 1974.